Bone Reports 12 (2020) 100281

Contents lists available at ScienceDirect

Bone Reports

journal homepage: www.elsevier.com/locate/bonr

Gnathodiaphyseal dysplasia is not recapitulated in a respective mouse model carrying a mutation of the Ano5 gene

Tim Rolvien[a,b,1], Osman Avci[a,1], Simon von Kroge[a], Till Koehne[a], Stefan Selbert[c,d], Stephan Sonntag[c,d], Doron Shmerling[c], Uwe Kornak[e,f,g], Ralf Oheim[a], Michael Amling[a], Thorsten Schinke[a], Timur Alexander Yorgan[a,*]

[a] Department of Osteology and Biomechanics, University Medical Center Hamburg-Eppendorf, Hamburg, Germany
[b] Department of Orthopedics, University Medical Center Hamburg-Eppendorf, Hamburg, Germany
[c] PolyGene AG, Rümlang, Switzerland
[d] ETH Phenomics Center (EPIC), ETH Zürich, Zürich, Switzerland
[e] Institute of Medical Genetics and Human Genetics, Charité-Universitätsmedizin Berlin, Berlin, Germany
[f] Berlin Brandenburg Center for Regenerative Therapies (BCRT), Charité-Universitätsmedizin Berlin, Berlin, Germany
[g] Max Planck Institute for Molecular Genetics, FG Development and Disease, Berlin, Germany

ARTICLE INFO

Keywords:
Ano5
Gnathodiaphyseal dysplasia
Mouse model
Skeletal disorder

ABSTRACT

Mutations in the gene *ANO5*, encoding for the transmembrane protein Anoctamin 5 (Ano5), have been identified to cause gnathodiaphyseal dysplasia (GDD) in humans, a skeletal disorder characterized by sclerosis of tubular bones, increased fracture risk and fibro-osseous lesions of the jawbones. To better understand the pathomechanism of GDD we have generated via Crispr/CAS9 gene editing a mouse model harboring the murine equivalent (Ano5 p.T491F) of a GDD-causing *ANO5* mutation identified in a previously reported patient. Skeletal phenotyping by contact radiography, μCT and undecalcified histomorphometry was performed in male mice, heterozygous and homozygous for the mutation, at the ages of 12 and 24 weeks. These mice did not display alterations of skeletal microarchitecture or mandible morphology. The results were confirmed in female mice and animals derived from a second, independent clone. Finally, no skeletal phenotype was observed in mice lacking ~40% of their *Ano5* gene due to a frameshift mutation. Therefore, our results indicate that Ano5 is dispensable for bone homeostasis in mice, at least under unchallenged conditions, and that these animals may not present the most adequate model to study the physiological role of Anoctamin 5.

1. Introduction

Mutations in the gene *ANO5* have been associated with the rare skeletal disorder gnathodiaphyseal dysplasia (GDD; OMIM: 166260) (Tsutsumi et al., 2004; Marconi et al., 2013; Rolvien et al., 2017). Indeed, *ANO5* (alternatively *TMEM16E*) was first identified in a Japanese family suffering from GDD, which led to the gene's original symbol GDD1 (Tsutsumi et al., 2004). Thereafter, several other patients were reported (Marconi et al., 2013; Rolvien et al., 2017; Duong et al., 2016; Jin et al., 2017; Otaify et al., 2018; Zeng et al., 2019; Marechal et al., 2019). GDD has an autosomal dominant inheritance pattern and is characterized by fibro-osseous lesions of the jawbones as well as sclerosis of tubular bones that have an increased fragility (Tsutsumi et al., 2004; Marconi et al., 2013; Rolvien et al., 2017; Mizuta et al., 2007). Additionally, homozygous or compound heterozygous loss-of-function mutations of *ANO5* have been reported to cause limb-girdle muscular dystrophy type 12 (OMIM: 611307) and Miyoshi muscular dystrophy 3 (OMIM: 613319) (Hicks et al., 2011; Schessl et al., 2012).

Despite this apparently crucial function in human physiology, there is little knowledge available with regard to the molecular function of Anoctamin 5. Ano5 belongs to the evolutionary highly conserved family of Anoctamins that comprises ten structurally similar proteins with eight transmembrane domains (Falzone et al., 2018). These members have however very divergent molecular functions, for instance as calcium-activated chloride channels, cation channels and phospholipid scramblases (Falzone et al., 2018). While the molecular function of

* Corresponding author at: Department of Osteology and Biomechanics, University Medical Center Hamburg Eppendorf, Martinistrasse 52, Hamburg 20246, Germany.
E-mail address: t.yorgan@uke.de (T.A. Yorgan).
[1] These authors contributed equally to this work.

https://doi.org/10.1016/j.bonr.2020.100281
Received 30 January 2020; Received in revised form 27 April 2020; Accepted 11 May 2020
Available online 14 May 2020

Ano5 has not been fully elucidated, its phylogenetically closest relative, Ano6, has been reported to exhibit all three of the prior mentioned molecular activities (Falzone et al., 2018; Pedemonte and Galietta, 2014). The function of Ano5 is further confounded by the observation that it is located in the cytoplasm and at the endoplasmic reticulum (Tsutsumi et al., 2004), in contrast to e.g. Ano6 that is located at the cell membrane (Ousingsawat et al., 2015). Only recently it was published that Ano5 displays a Ca^{2+}-activated phospholipid scramblase activity in in vitro systems and that mutations linked to GDD cause a gain-of-function in scramblase activity (Yu et al., 2015; Gyobu et al., 2016; Di Zanni et al., 2018; Di Zanni et al., 2020). Importantly however, the full physiological function of Ano5 remains ill-defined and enigmatic.

With regard to this issue, the muscular and skeletal phenotype of *Ano5*-deficient mice was recently described (Xu et al., 2015; Wang et al., 2019). While the loss of Ano5 did not recapitulate the myopathies (Xu et al., 2015), some aspects of GDD were identified in the skeleton of *Ano5*-deficient mice (Wang et al., 2019). In detail, the authors observed a marked increase in cortical thickness and moderately increased bone matrix mineralization as well as indicators of periodontal inflammation and slightly enlarged and denser mandibles. The latter symptom is however far more severe in GDD patients. Moreover, the trabecular bone volume of the *Ano5*-deficient mice was reduced, in contrast to GDD patients that display sclerosing of the trabecular compartment (Rolvien et al., 2017). Since a complete loss of gene function might convey a fundamentally different effect than a point mutation potentially causing a gain-of-function, we believe it is highly important to establish an animal model of GDD carrying a specific mutation in order to understand the pathomechanism and ultimately improve treatment options for the affected patients.

We recently reported a novel *ANO5* mutation (p.Ser500Phe), located the second extracellular loop of the protein and identified in a 13-year-old male patient, displaying the hallmark symptoms of GDD (Rolvien et al., 2017; Di Zanni et al., 2020). Closer analysis of the skeletal phenotype revealed a systemic high bone turnover, increased bone mass and recurring pathological fractures. Since mice are a well-established animal model with excellent transferability of findings in the musculoskeletal system, we have generated the first mouse model carrying a specific GDD-causing mutation based on the case of this patient. Our data obtained by skeletal phenotyping clearly demonstrate that the murine equivalent of the human mutation does not transfer the GDD pathology into the mouse model.

2. Materials & methods

2.1. Clinical assessments

Follow-up data and additional clinical assessment of a previously reported GDD patient is described (Rolvien et al., 2017). In this patient, additional computed tomography (CT) of both legs had been carried out. Dual-energy X-ray Absorptiometry (DXA) equipped with a pediatric software (Lunar iDXA; GE Healthcare, USA) was carried out at one and three years follow-up; and age-adjusted *Z*-scores were calculated by the software. We also assessed bone microstructural parameters including cortical thickness (Ct.Th) using high-resolution peripheral quantitative computed-tomography (HR-pQCT, Scanco Medical, Switzerland) at the distal tibia as described previously (Rolvien et al., 2017). Informed consent was obtained from the patient and his parents according to the rules of the local ethics committee of the University Medical Center Hamburg-Eppendorf, Germany.

2.2. Generation of the Ano5-KI and Ano5-KO mouse lines via Crispr/CAS9

Mouse lines with modified *Ano5* genes were generated by PolyGene AG, Switzerland. Two synthetic sgRNA target sequences (GGCTTCGC TTTCCATGAAGCTGG and GAAGCTCTTCACGCTCTGCAGGG) and a 198 nt donor DNA oligonucleotide with the mutations located in the middle were chosen to localize to the site of the mutation observed in the patients using crispr.mit.edu (Hsu et al., 2013). Pronuclear injection of both sgRNAs, the donor DNA and Cas9 protein (Biolabs, M0641T) was injected into single cell stage embryos obtained from superovulated C57Bl/6N mice according to standard protocols. Injected embryos were implanted into foster mothers.

Genotyping was performed via PCR amplification (forward primer: AGATCTCAGGCCCATGGAGCAG; reverse primer: ATGGCTAAGGAGTC CTGAAC) and subsequent Sanger sequencing (Seqlab- Microsynth GmbH, Germany) using the forward primer. Potential off-target effects were excluded at sites identified by the algorithm from http://crispor.tefor.net/ (Haeussler et al., 2016).

Two mice harboring all intended mutations were chosen to establish two independent colonies (B6-*Ano5*^{tm1Pg}/Uke and B6-*Ano5*^{tm2Pg}/Uke).

A mouse with a single nucleotide insertion causing a frame shift and subsequent premature stop codon was chosen to establish the *Ano5*-deficient mouse line (B6-*Ano5*^{tm3Pg}/Uke).

2.3. Animal husbandry and experiments

All mice were kept in a specific pathogen-free environment with a 12-hour light/dark cycle, 45–65% relative humidity and 20–24 °C ambient temperature in open or individually ventilated cages with wood shavings bedding and nesting material in groups not surpassing 6 animals. The mice had access to tap water and standard rodent chow (1328P, Altromin Spezialfutter GmbH & Co. KG, Germany) ad libitum. All animal experiments were performed according to the Cantonal Veterinary of the Canton of Zurich, Swiss Federal Animal Welfare Law TSchG, Art. 11.1, Animal Welfare Regulations, Art. 142, Animal Experimentation Regulations, Art 9 and Annex 1 or were approved by the animal facility of the University Medical Center Hamburg-Eppendorf and by the "Behörde für Soziales, Familie, Gesundheit und Verbraucherschutz" (Org869) in accordance with the local implementation of EU Directive 2010/63/EU for animal experiments.

2.4. Radiological assessment

The animals were sacrificed via CO_2 intoxication and the skeletons were fixed in 3.7% PBS-buffered formaldehyde for 48 h and subsequently stored in 80% ethanol. The dental status was assessed by contact radiography (35 kV, 2 s) of the left mandible in an X-ray cabinet (Faxitron Xray Corp., USA).

μCT scanning and microarchitectural analysis was performed with a voxel resolution of 10 μm using a μCT 40 desktop cone-beam microCT (Scanco Medical, Switzerland) as previously described (Yorgan et al., 2015) according to standard guidelines(Bouxsein et al., 2010). Trabecular bone was analyzed in the distal metaphysis of the femur in a volume situated 2500 μm to 500 μm proximal of the distal growth plate with a threshold of 250. Cortical bone was analyzed in a volume with a length of 1000 μm situated in the middle of the femoral diaphysis with a threshold of 300.

2.5. Mouse histology (bone and muscle)

For bone histology, the fixed lumbar vertebral bodies L1 to L4 were dehydrated in ascending alcohol concentrations and then embedded in methylmetacrylate as described previously (Keller et al., 2014). Sections of 4 μm thickness were cut in the sagittal plane on a Microtec rotation microtome (Techno-Med GmbH, Germany). These were stained by the von Kossa/van Gieson or Toluidine blue staining procedure as previously described (Albers et al., 2013). Histomorphometry was performed according to the ASBMR guidelines (Dempster et al., 2013) using the Bioquant Osteo histomorphometry system (BIOQUANT Image Analysis Corp., USA) for trabecular bone micorachitecture analysis. For cellular and dynamic histomorphometry, the Osteomeasure system (Osteometrics Inc., USA) was utilized.

For muscle histology the gastrocnemius muscle was embedded in paraffin and sectioned in the transversal plane. After haematoxylin and eosin staining the myofiber size was assessed on sections obtained from the widest cross section of the muscle using the ImageJ software (Schneider et al., 2012) by manual tracing of individual myofibers.

2.6. Mechanical testing

Destructive three point bending tests utilizing a BZ2.5 materials testing machine and the testXpert software (both ZwickRoell GmbH & Co. KG, Germany) were performed on explanted femora as described previously (Luther et al., 2018). In brief, support bar spacing was 7 mm and a tip was lowered at a constant speed of 2 mm/min until failure. All presented parameters were calculated within the software from the recorded distance and force.

2.7. Expression analysis

RNA from the gastrocnemius muscle of 24 week old mice was isolated via TriFast extraction (VWR International, LLC, USA). For qRT-PCR expression analysis 500 ng of RNA was reversed transcribed with oligo-dT primers using the Verso cDNA Kit (Thermo Fisher Scientific Inc., USA) according to manufacturer's instructions. Predesigned TaqMan assays (Thermo Fisher Scientific Inc., USA) and Taqman gene expression mastermix (Thermo Fisher Scientific Inc., USA) were used to assess the expression of *Ano5* (Mm00624629_m1) and *Gapdh* (Mm99999915_g1) as an internal control. Quantification relative to Gapdh was applied for individual samples.

2.8. Biomarker analysis

For the determination of organ damage biomarkers, serum of the sacrificed mice was collected immediately post mortem. Quantification was performed using antibody-based or enzyme activity-based detection kits (Alkaline phosphatase (ALP): Cusabio Technology LLC, USA, MBS703336; lactate: BioAssay Systems, USA, ECLC-100; B-type natriuretic peptide (BNP): Sigma-Aldrich, USA, RAB0386; alanine transaminase (ALT), Sigma-Aldrich, USA, MAK052; aspartate transaminase (AST), Sigma-Aldrich, USA, MAK055) according to the manufacturers' instructions.

2.9. Statistical analysis

All data presented in the manuscript are presented as individual values and as means ± standard deviations. Statistical analysis was performed via unpaired, two-tailed Student's *t*-test with Bonferroni correction for multiple testing using Prism software (GraphPad Software, USA). P-values below 0.05 were considered statistically significant. Sample size and power of analysis for animal experiments was determined by an a priori *t*-test with G*Power (Faul et al., 2007).

3. Results

We have previously reported the case of a GDD patient presenting with the hallmark clinical characteristics of GDD, such as cemento-osseous lesions of the jawbone and osteosclerosis of long bones associated with recurrent, bilateral diaphyseal femur fractures, which had previously been treated by intramedullary nail fixation (Fig. 1A) (Rolvien et al., 2017). During follow-up, one additional metatarsal fracture had occurred. While the BMD *Z*-score determined by DXA remained constant (Fig. 1B), cortical thickness assessed by HR-pQCT at the distal tibia further increased at one and three years follow-up, which led to values clearly above the age-adjusted reference values from the literature (Fig. 1C) (Nishiyama et al., 2012). These clinical data demonstrate the progressive nature and lack of viable treatment options for this disorder and highlight the necessity for representative disease models.

A mouse line harboring the murine equivalent of the *ANO5* mutation c.1499C > T (p.S500F) observed in this GDD patient was generated by Crispr/CAS9 based DNA modification of murine pronuclei. A single strand donor DNA oligomer was used as a template to introduce five point mutations. The mutations c.1471A > T and c.1472C > T were designed to facilitate the desired p.T491F amino acid exchange and the additional mutations c.1449C > T, c.1470C > T and c.1474C > T are translationally silent but were designed to modify the PAM sites recognized by the guide RNA, thus reducing the probability of mutation reversal after the initial modification (Fig. 1D). Genotyping of the mice was performed via Sanger sequencing and thereby we were also able to confirm the successful introduction of all intended mutations (Fig. 1E).

In order to examine the skeletal phenotype of mice harboring the $Ano5^{KI}$ allele, we first analyzed the structural microarchitecture of the trabecular bone compartment in the distal femoral metaphysis. We focused our investigations on male mice, since this reflects the reported patient's gender. Surprisingly, neither the $Ano5^{+/KI}$ mice, with a zygosity equivalent to the patient, nor the $Ano5^{KI/KI}$ mice displayed any significant differences in their trabecular architecture and mineral content towards $Ano5^{+/+}$ littermate controls at the age of 12 or 24 weeks (Fig. 2A,B). Similarly, we did not observe significant differences in the cortical parameters determined at the mid-diaphysis of femora from 12 and 24 weeks old, $Ano5^{+/KI}$ or $Ano5^{KI/KI}$ male mice. Indeed, in addition to the cortical thickness, cortical porosity and the midshaft diameter, the cortical tissue mineral density was unaltered as well (Fig. 3A,B).

We extended our investigations by including structural histomorphometry of undecalcified vertebral sections. Here we found that the introduced mutation within the *Ano5* gene did not affect the trabecular architecture in the vertebral bodies of 12 and 24 weeks old $Ano5^{+/KI}$ or $Ano5^{KI/KI}$ mice (Fig. 4A,B). Moreover, the investigation of cellular and dynamic parameters revealed no significant differences indicative of an altered bone turnover (Fig. 4C). In line with these data, three point bending tests of femora from $Ano5^{+/KI}$ and $Ano5^{KI/KI}$ mice showed that the mechanical properties were not significantly different from $Ano5^{+/+}$ control mice (Suppl. Fig. 1). In order to exclude potential sexual dimorphisms, we additionally analyzed the skeletal microarchitecture of 12 weeks old female $Ano5^{+/KI}$ and $Ano5^{KI/KI}$ mice. In line with the results obtained in male mice, female mice carrying this *Ano5* mutation did not display significant differences in any of the investigated structural parameters (Suppl. Fig. 2A–C). Furthermore, to exclude epistatic off-target effects that could potentially have been introduced by the CAS9 endonuclease, we additionally analyzed the skeletal structure of a mouse line generated from an independent pronucleus injection. While this line carried the desired *Ano5* mutations as well, heterozyogous mutant mice did not display any structural changes in their skeletal architecture (Suppl. Fig. 3A–C).

Given that fibro-osseous lesions of the jawbones are a hallmark of GDD (Tsutsumi et al., 2004; Rolvien et al., 2017), we examined the mandibles of $Ano5^{+/KI}$ and $Ano5^{KI/KI}$ mice by radiography. Similar to the previous results, there were no detectable dental abnormalities observed in these mice (Suppl. Fig. 4A). Since mutations of the *ANO5* gene in humans have also been associated with muscular dystrophies including limb-girdle muscular dystrophy type 12 (OMIM: 611307) and Miyoshi muscular dystrophy 3 (OMIM: 613319) (Hicks et al., 2011; Schessl et al., 2012), we further examined the muscular phenotype of the $Ano5^{+/KI}$ and $Ano5^{KI/KI}$ at the gastrocnemius muscle. Here, only in 24 weeks old $Ano5^{KI/KI}$ mice a small but significant increase in relative muscle mass was observed. However, the histological analysis of individual myofibres revealed comparable myofibre cross-sectional areas for all genotypes in 12 and 24 weeks old mice (Suppl. Fig. 4B,C). Furthermore, the assessment of serum biomarkers of general (ALP and lactate) or specific (BNP, ALT, AST) organ damage in 12 and 24 weeks old mice did not reveal significant differences between the genotypes

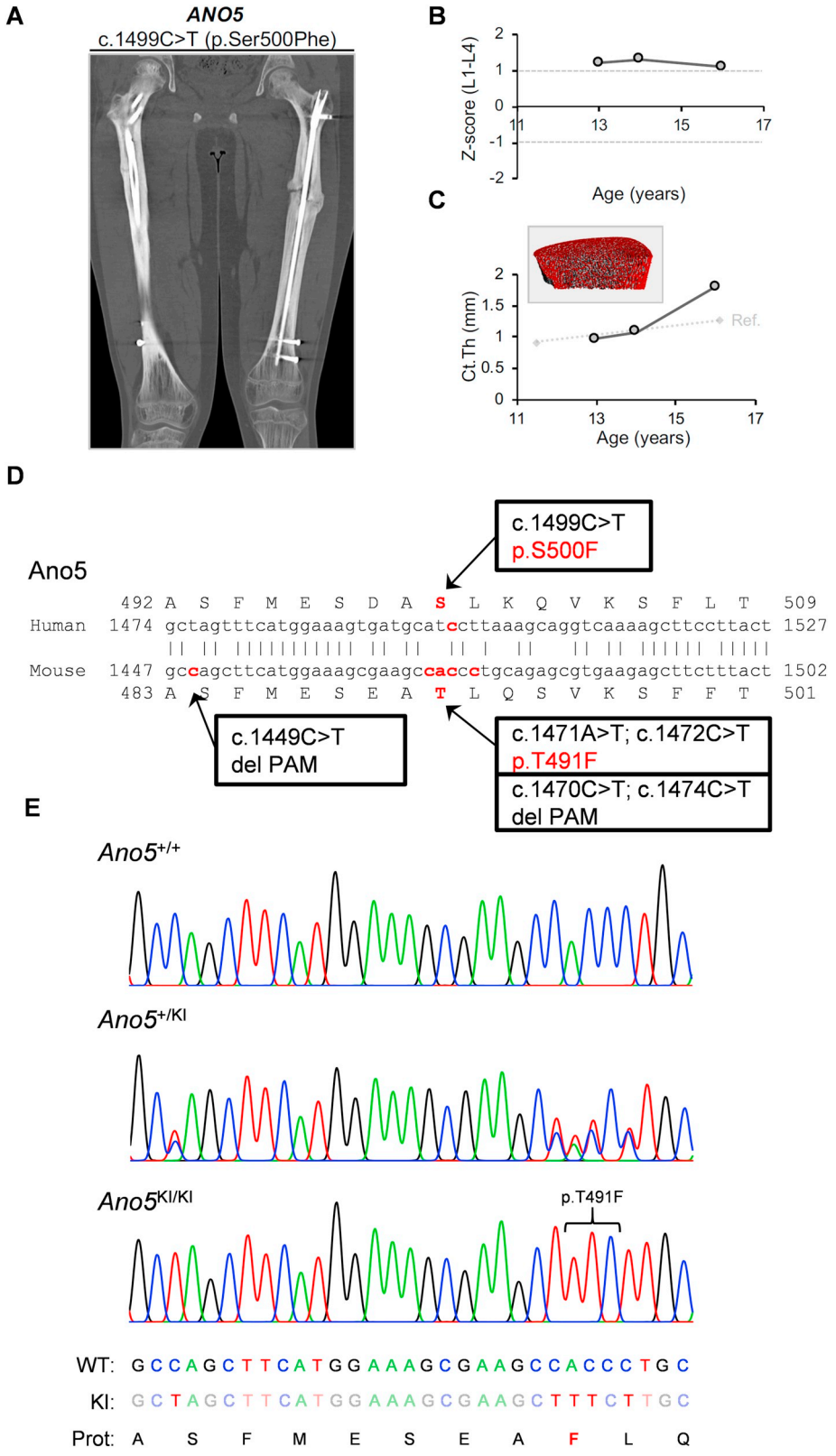

Fig. 1. Clinical follow-up of the previously reported GDD patient (*ANO5* c.1499C > T (p.S500F) (Rolvien et al., 2017)) and generation of the corresponding *Ano5*^{KI} mouse line. A) Computed tomography (coronal reformat) showing bilateral diaphyseal femur fractures previously treated by intramedullary nail fixation. Note the post-traumatic femur length discrepancy and the pronounced cortical thickening of the femoral diaphysis. B) Unchanged, slightly elevated BMD *Z*-scores at follow-up assessed by DXA at the lumbar spine (L1–4). C) Increase of cortical thickness determined by HR-pQCT at the distal tibia compared to age-matched reference values (Ref. (Nishiyama et al., 2012)). D) Sequence comparison between the mutated human and murine *Ano5* gene. The mutations are indicated in red letters. Additional silent mutations have been introduced into the murine *Ano5* gene to disrupt the PAM sites and prevent mutation reversal. E) Sanger sequencing chromatograms of the modified genetic region in wildtype, heterozygous and homozygous mice. The bracket indicates the p.T491F amino acid change.

(Suppl. Fig. 4D), suggesting that no major pathological alterations are present in other organs.

Finally, as a side product of the Crispr/CAS9 method utilized to generate the mouse lines harboring the specific mutation, we additionally obtained a clone with a mutation (c.1478insA) resulting in a premature stop codon (p.(Ser494GlufsTer32)) and consequently a loss of approximately 40% of the gene product at the C-terminal end (Fig. 5A,B). This allele results in a truncated protein, designated *Ano5*^{KO} and was considered deleterious (PROVEAN score: −1288.598) (Choi et al., 2012). Indeed, expression of *Ano5* in the gastrocnemius muscle of *Ano5*$^{KO/KO}$ mice was severely reduced (Fig. 5C). Skeletal analysis of female *Ano5*$^{+/KO}$ and *Ano5*$^{KO/KO}$ mice at the age of 12 weeks revealed

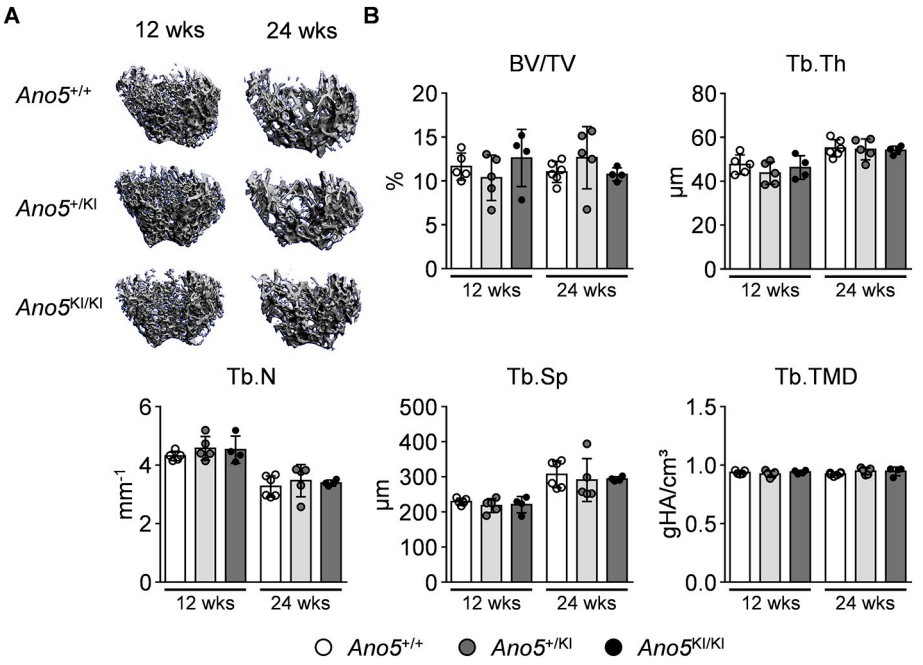

Fig. 2. Trabecular microarchitecture of *Ano5*^{KI} mice. A) Representative µCT reconstructions of the distal femoral trabecular bone compartment of 12 and 24 week old male mice. B) µCT-based quantification of microarchitectural parameters of the trabecular bone compartment in the distal femoral metaphysis of male *Ano5*$^{+/+}$, *Ano5*$^{+/KI}$ and *Ano5*$^{KI/KI}$ mice at the indicated ages. Data were analyzed by Student's *t*-test with Bonferroni correction. Group sizes are indicated by the individual data points. *P < 0.05 vs. *Ano5*$^{+/+}$ of the same age.

the presence of a very mild phenotype. While microarchitectural parameters were not affected, *Ano5*$^{KO/KO}$ mice displayed a significantly increased tissue mineral density in the trabecular and cortical compartment as well as reduced cortical porosity in comparison to *Ano5*$^{+/+}$ littermates as determined by µCT evaluation of the femora (Fig. 5D–F).

4. Discussion

In humans, mutations in the gene *ANO5* can lead to gnathodiaphyseal dysplasia, a rare skeletal disorder and muscular dystrophies (Tsutsumi et al., 2004; Marconi et al., 2013; Rolvien et al., 2017; Hicks et al., 2011; Schessl et al., 2012), indicating an essential function of Anoctamin 5 in human musculoskeletal physiology. Despite this apparent relevance, the molecular function of Ano5 is still not fully elucidated. In an attempt to address this issue and to provide a suitable model to study the pathomechanism of GDD, we have generated a mouse line harboring the murine equivalent of a mutation that was observed in a recently described GDD patient (Rolvien et al., 2017). This 13-year-old male patient suffered from increased fragility of the appendicular skeleton and osseous lesions in the mandible.

The mouse model harboring the p.T491F mutation (equivalent to the human p.S500F mutation) was successfully generated using Crispr/CAS9 gene editing. While this residue is not completely evolutionarily conserved, most vertebrates harbor either a serine (e.g. humans) or a biochemically closely related threonine (e.g. mice) at this position. Indeed, it has recently been suggested that, in contrast to those mutations causing muscular dystrophies, GDD-causing mutations of *ANO5* convey a gain of function (Di Zanni et al., 2018; Di Zanni et al., 2020). Among other mutations, this was also shown for the pS500F mutations analyzed in this study. Interestingly, all mutations investigated in the aforementioned studies did not appear to influence the cellular localization of the Ano5 protein.

Although GDD is an autosomal dominant disorder, we additionally analyzed mice homozygous for the mutant allele throughout this study to provide further strength for our results. Careful evaluation revealed

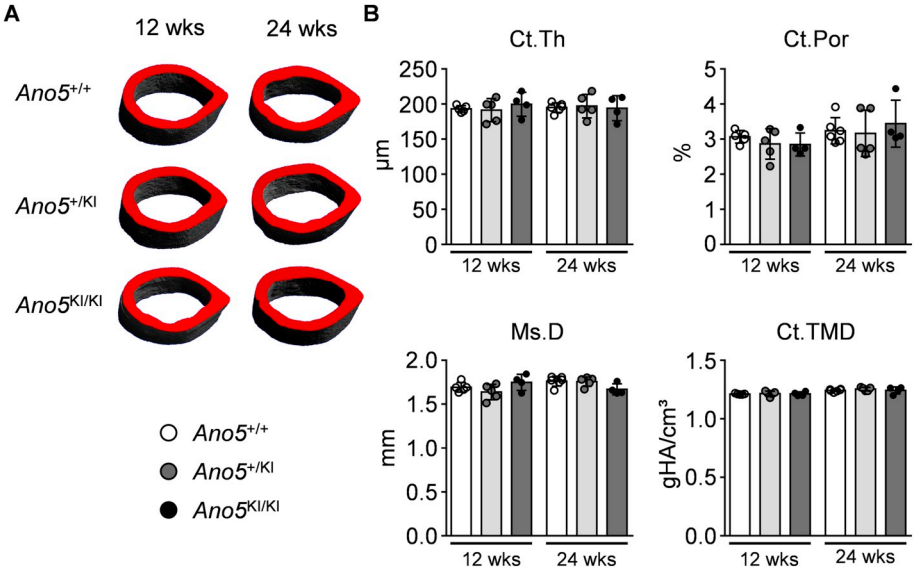

Fig. 3. Cortical microarchitecture of *Ano5*^{KI} mice. A) Representative µCT reconstructions of the femoral diaphysis of 12 and 24 week old male mice. B) µCT-based quantification of microarchitectural parameters of the mid-diaphyseal cortical bone of male *Ano5*$^{+/+}$, *Ano5*$^{+/KI}$ and *Ano5*$^{KI/KI}$ mice at the indicated ages. Data were analyzed by Student's *t*-test with Bonferroni correction. Group sizes are indicated by the individual data points.

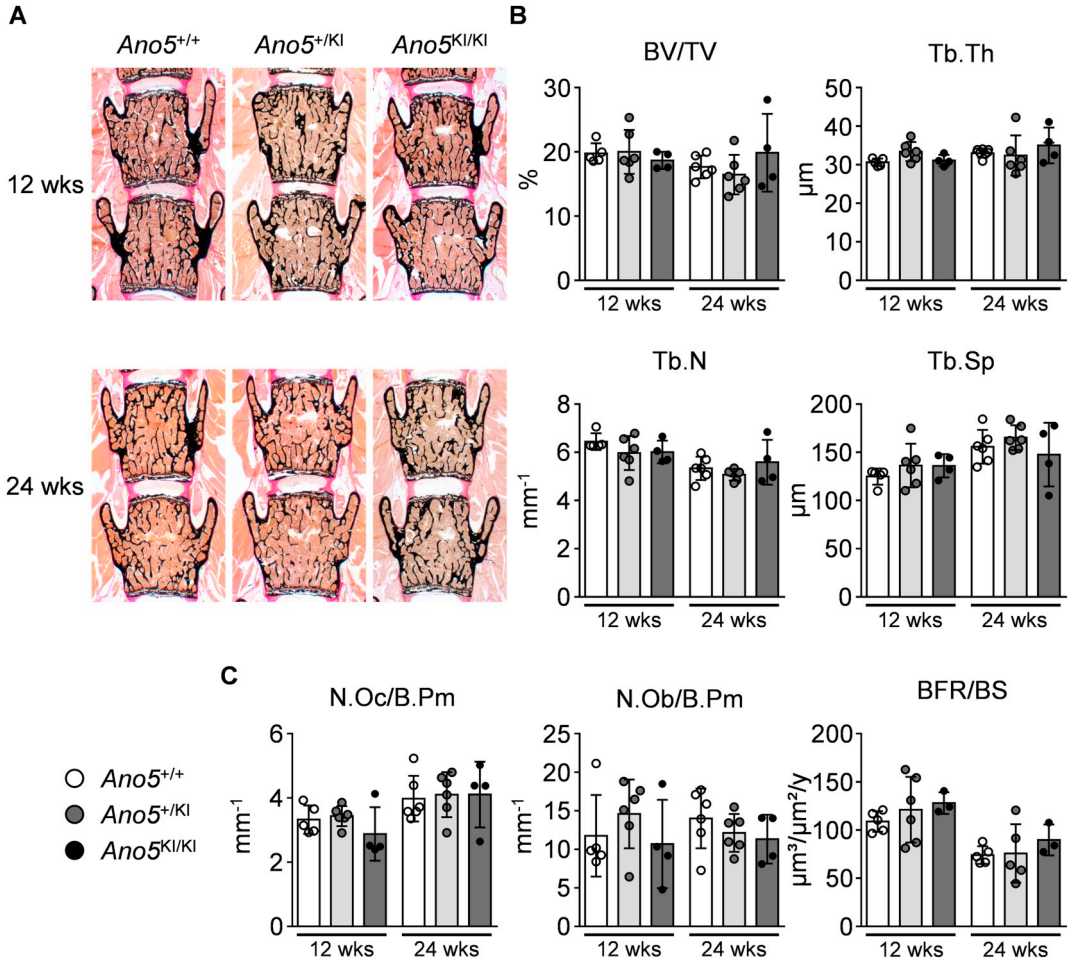

Fig. 4. Undecalcified histology of vertebral bodies from *Ano5*^{KI} mice. A) Representative undecalcified histological sections of vertebral bodies L3 and L4 from 12 and 24 week old, male *Ano5*$^{+/+}$, *Ano5*$^{+/KI}$ and *Ano5*$^{KI/KI}$ mice. Von Kossa/van Gieson stain. B) Histomorphometric evaluation of the trabecular microarchitecture in the vertebral bodies of male *Ano5*$^{+/+}$, *Ano5*$^{+/KI}$ and *Ano5*$^{KI/KI}$ mice at the indicated ages. C) Histomorphometric evaluation of the trabecular cellular and kinetic parameters in the vertebral bodies of male *Ano5*$^{+/+}$, *Ano5*$^{+/KI}$ and *Ano5*$^{KI/KI}$ mice at the indicated ages. Data were analyzed by Student's *t*-test with Bonferroni correction. Group sizes are indicated by the individual data points.

that neither *Ano5*$^{+/KI}$ nor *Ano5*$^{KI/KI}$ mice displayed hallmark features of GDD. More specifically, there were no significant changes in the skeletal microarchitecture and cellular composition in comparison to wildtype littermates, neither in the femora nor in the vertebral bodies of these mice. Furthermore, none of the mice displayed anomalies in their mandibles, therefore excluding the presence of the severe osseous lesions observed in the patient. Finally, neither the *Ano5*$^{+/KI}$ nor the *Ano5*$^{KI/KI}$ mice displayed a muscular phenotype at the gastrocnemius muscle that would indicate any type of myopathy. The same observations were also made in female mice, thus excluding gender-specific effects. Although unlikely, the Crispr/CAS9 gene editing tools used to generate this mouse line might have introduced epistatic off-target modifications masking the effect of the mutated *Ano5* allele. To rule out this possibility, we also analyzed offspring from a second, independently generated mouse line, but again no skeletal phenotype was detected.

Furthermore, we were able to assess the function of Ano5 in skeletal metabolism in a more general and potentially opposing manner, since we additionally generated a mouse line harboring a frameshift mutation resulting in a premature stop codon and the loss of approximately 40% of the gene product on the C-terminal side. Although the activity of the truncated Ano5 was not directly assessed in the context of this study, an in silico prediction deemed this mutations to be deleterious. Additionally, the expression of *Ano5* was nearly absent, most likely due to nonsense mediated decay. Similar to the lines carrying the *Ano5*^{KI} allele, these mice did not display a skeletal phenotype as well. These results indicate that reduced expression levels of Ano5 as a potential consequence of mutations are not relevant in mice.

Our data that show no obvious physiological effect caused by the modifications of *Ano5* are in line with results recently reported for *Ano5*-deficient mice, where an absence of a muscular phenotype under physiological conditions was described (Xu et al., 2015). These results are seemingly counter-intuitive to the reported high expression of *Ano5* in the musculoskeletal tissue of mice (Xu et al., 2015), however a potential explanation might be related to a potential function of Ano5. In fact, it has been suggested, based on phenotypic similarities between *ANO5* associated muscular dystrophies and dysferlinopathies, that Ano5 might be involved in the process of membrane repair (Bolduc et al., 2010). Therefore it is conceivable that the function of Ano5 is only required, if there is cell membrane damage. Potentially, a challenge, such as muscular training, is required to induce an observable phenotype that is not present under homeostatic conditions. Indeed, muscles from *Ano5*-deficient mice have been shown to display a reduced repair response to laser-induced injury (Griffin et al., 2016). Furthermore, this result was recently confirmed in patient-derived *ANO5*-deficient human muscle cells (Chandra et al., 2019).

However, it has to be noted that our results are in apparent contradiction to another study, where *Ano5*-deficient mice recapitulated some aspects of GDD (Wang et al., 2019). We can only speculate on the discrepancy between our data and the previously reported results. It is

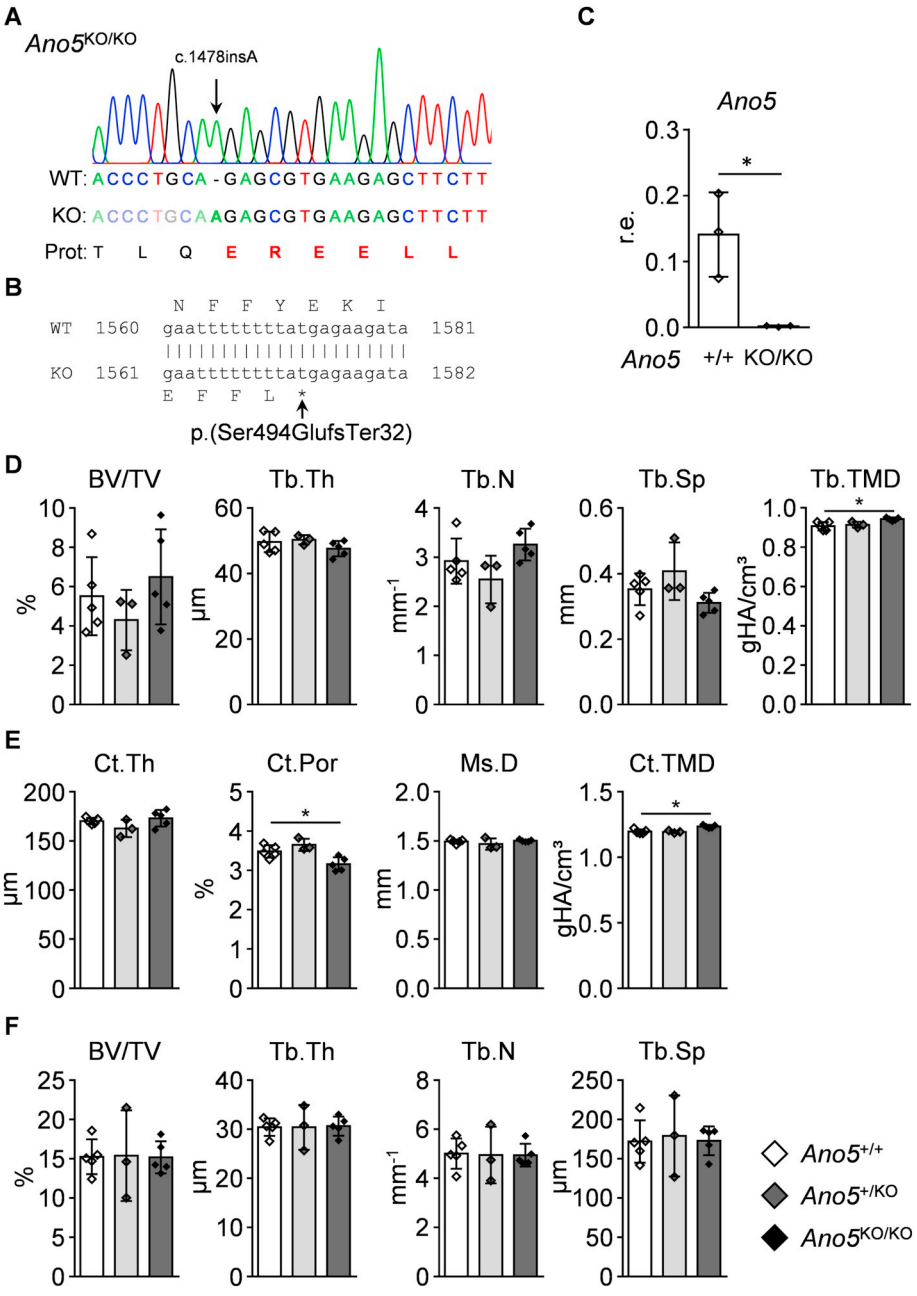

Fig. 5. Skeletal phenotyping of *Ano5*-deficient mice. A) Sanger sequencing chromatogram representing the altered genomic sequence. The arrow indicates the inserted nucleotide and the altered protein sequence is indicated by red, bold letters. B) Comparison of the wildtype and mutated *Ano5* gene sequence in the region, where the frame shift leads to a premature stop codon. C) qRT-PCR based expression analysis of *Ano5* in the gastrocnemius muscle of 24 week old *Ano5*$^{+/+}$ and *Ano5*$^{KO/KO}$ mice. Expression levels are relative to *Gapdh*. D) µCT based analysis of the trabecular bone in the distal femoral metaphysis of 12 week old female *Ano5*$^{+/+}$, *Ano5*$^{+/KO}$ and *Ano5*$^{KO/KO}$ mice. E) µCT based analysis of the cortical bone in the femoral mid-diaphysis of 12 week old female *Ano5*$^{+/+}$, *Ano5*$^{+/KO}$ and *Ano5*$^{KO/KO}$ mice. F) Histomorphometric evaluation of the trabecular microarchitecture in the L3 and L4 vertebral bodies of 12 week old female *Ano5*$^{+/+}$, *Ano5*$^{+/KO}$ and *Ano5*$^{KO/KO}$ mice. Data were analyzed by Student's *t*-test with Bonferroni correction. Group sizes are indicated by the individual data points. *P < 0.05 vs. *Ano5*$^{+/+}$.

conceivable that our deficiency model retains some residual function that might mitigate the effects of a complete loss of the gene. Likewise, although very similar strategies were chosen, minor methodological differences might partially account for the observed differences. Nonetheless, it is quite surprising that a loss of *Ano5* mimics the phenotype of GDD, especially in the light of the aforementioned study suggesting that GDD-causing mutations convey a gain-of-function (Di Zanni et al., 2018; Di Zanni et al., 2020). Additionally, only very limited data was provided on mice with heterozygous deletion of *Ano5* (Wang et al., 2019), although GDD is a autosomal dominant disorder. Therefore, we believe that further research is required to resolve this apparent contradiction.

Our results add to the growing body of evidence elucidating the physiological role of Anoctamin 5 and contain the first reported data on a mouse model harboring a specific GDD-associated mutation of *Ano5*. In line with the recently reported lack of an obvious muscular phenotype in *Ano5*-deficient mice, and in contrast to a recent study assessing the skeletal phenotype of *Ano5*-deficient mice (Xu et al., 2015; Wang et al., 2019), our results provide further indication that, *Ano5* is dispensable for the homeostasis of the musculoskeletal system in mice. Therefore, we believe that mice are not the most adequate model to study the physiological function of Anoctamin 5 under homeostatic conditions, especially with regard to human diseases.

Supplementary data to this article can be found online at https://doi.org/10.1016/j.bonr.2020.100281.

Transparency document

The Transparency document associated with this article can be found, in online version.

Grant supporters

This project has received funding from the European Community's Seventh Framework Programme under grant agreement no. 602300 (SYBIL).

CRediT authorship contribution statement

Tim Rolvien:Methodology, Investigation, Writing - review & editing, Visualization.**Osman Avci**:Methodology, Investigation, Writing - review & editing, Visualization.**Simon von Kroge** Investigation, Writing - review & editing.**Till Koehne**:Investigation, Writing - review & editing.**Stefan Selbert**:Methodology, Investigation, Writing - review & editing.**Stephan Sonntag**:Methodology, Investigation, Writing - review & editing.**Doron Shmerling**:Conceptualization, Methodology, Resources, Writing - review & editing.**Uwe Kornak**: Conceptualization, Writing - review & editing.**Ralf Oheim**: Conceptualization, Writing - review & editing.**Michael Amling**: Conceptualization, Resources, Writing - review & editing, Funding acquisition.**Thorsten Schinke**:Conceptualization, Resources, Writing - review & editing, Supervision, Funding acquisition.**Timur Alexander Yorgan**:Conceptualization, Methodology, Formal analysis, Writing - original draft, Writing - review & editing, Visualization, Supervision.

Declaration of competing interest

The authors declare no conflict of interest.

Acknowledgements

We would like to thank the UKE research animal facility for their services. Moreover we would like to express our gratitude to Lana Rosenthal, Olga Winter, Mona Neven Elke Leicht, Andrea Thieke and Annica Pröhl for their technical assistance.

Authors' roles: Study design: DS, UK, RO, MA, TS, TAY. Study conduct: TR, OA, SvK, TK, SS, SS, TAY. Data interpretation: TR, OA, UK, RO, MA, TS, TAY. Drafting manuscript: TR, TS, TAY. Revising manuscript: all authors. Approving manuscript for publication: all authors.

References

Albers, J., Keller, J., Baranowsky, A., Beil, F.T., Catala-Lehnen, P., Schulze, J., Amling, M., Schinke, T., 2013. Canonical Wnt signaling inhibits osteoclastogenesis independent of osteoprotegerin. J. Cell Biol. 200 (4), 537–549.

Bolduc, V., Marlow, G., Boycott, K.M., Saleki, K., Inoue, H., Kroon, J., Itakura, M., Robitaille, Y., Parent, L., Baas, F., Mizuta, K., Kamata, N., Richard, I., Linssen, W.H., Mahjneh, I., de Visser, M., Bashir, R., Brais, B., 2010. Recessive mutations in the putative calcium-activated chloride channel Anoctamin 5 cause proximal LGMD2L and distal MMD3 muscular dystrophies. Am. J. Hum. Genet. 86 (2), 213–221.

Bouxsein, M.L., Boyd, S.K., Christiansen, B.A., Guldberg, R.E., Jepsen, K.J., Muller, R., 2010. Guidelines for assessment of bone microstructure in rodents using micro-computed tomography. J. Bone Miner. Res. 25 (7), 1468–1486.

Chandra, G., Defour, A., Mamchoui, K., Pandey, K., Mishra, S., Mouly, V., Sreetama, S., Mahad Ahmad, M., Mahjneh, I., Morizono, H., Pattabiraman, N., Menon, A.K., Jaiswal, J.K., 2019. Dysregulated calcium homeostasis prevents plasma membrane repair in Anoctamin 5/TMEM16E-deficient patient muscle cells. Cell Death Dis. 5, 118.

Choi, Y., Sims, G.E., Murphy, S., Miller, J.R., Chan, A.P., 2012. Predicting the functional effect of amino acid substitutions and indels. PLoS One 7 (10), e46688.

Dempster, D.W., Compston, J.E., Drezner, M.K., Glorieux, F.H., Kanis, J.A., Malluche, H., Meunier, P.J., Ott, S.M., Recker, R.R., Parfitt, A.M., 2013. Standardized nomenclature, symbols, and units for bone histomorphometry: a 2012 update of the report of the ASBMR Histomorphometry Nomenclature Committee. J. Bone Miner. Res. 28 (1), 2–17.

Di Zanni, E., Gradogna, A., Scholz-Starke, J., Boccaccio, A., 2018. Gain of function of TMEM16E/ANO5 scrambling activity caused by a mutation associated with gnathodiaphyseal dysplasia. Cell. Mol. Life Sci. 75 (9), 1657–1670.

Di Zanni, E., Gradogna, A., Picco, C., Scholz-Starke, J., Boccaccio, A., 2020. TMEM16E/ANO5 mutations related to bone dysplasia or muscular dystrophy cause opposite effects on lipid scrambling. Hum. Mutat. 41 (6), 1157–1170.

Duong, H.A., Le, K.T., Soulema, A.L., Yueh, R.H., Scheuner, M.T., Holick, M.F., Christensen, R., Tajima, T.L., Leung, A.M., Mallya, S.M., 2016. Gnathodiaphyseal dysplasia: report of a family with a novel mutation of the ANO5 gene. Oral Surg. Oral Med. Oral Pathol. Oral Radiol. 121 (5), e123–e128.

Falzone, M.E., Malvezzi, M., Lee, B.C., Accardi, A., 2018. Known structures and unknown mechanisms of TMEM16 scramblases and channels. J. Gen. Physiol. 150 (7), 933–947.

Faul, F., Erdfelder, E., Lang, A.G., Buchner, A., 2007. G*power 3: a flexible statistical power analysis program for the social, behavioral, and biomedical sciences. Behav. Res. Methods 39 (2), 175–191.

Griffin, D.A., Johnson, R.W., Whitlock, J.M., Pozsgai, E.R., Heller, K.N., Grose, W.E., Arnold, W.D., Sahenk, Z., Hartzell, H.C., Rodino-Klapac, L.R., 2016. Defective membrane fusion and repair in Anoctamin5-deficient muscular dystrophy. Hum. Mol. Genet. 25 (10), 1900–1911.

Gyobu, S., Miyata, H., Ikawa, M., Yamazaki, D., Takeshima, H., Suzuki, J., Nagata, S., 2016. A role of TMEM16E carrying a scrambling domain in sperm motility. Mol. Cell. Biol. 36 (4), 645–659.

Haeussler, M., Schonig, K., Eckert, H., Eschstruth, A., Mianne, J., Renaud, J.B., Schneider-Maunoury, S., Shkumatava, A., Teboul, L., Kent, J., Joly, J.S., Concordet, J.P., 2016. Evaluation of off-target and on-target scoring algorithms and integration into the guide RNA selection tool CRISPOR. Genome Biol. 17 (1), 148.

Hicks, D., Sarkozy, A., Muelas, N., Koehler, K., Huebner, A., Hudson, G., Chinnery, P.F., Barresi, R., Eagle, M., Polvikoski, T., Bailey, G., Miller, J., Radunovic, A., Hughes, P.J., Roberts, R., Krause, S., Walter, M.C., Laval, S.H., Straub, V., Lochmuller, H., Bushby, K., 2011. A founder mutation in Anoctamin 5 is a major cause of limb-girdle muscular dystrophy. Brain 134 (Pt 1), 171–182.

Hsu, P.D., Scott, D.A., Weinstein, J.A., Ran, F.A., Konermann, S., Agarwala, V., Li, Y., Fine, E.J., Wu, X., Shalem, O., Cradick, T.J., Marraffini, L.A., Bao, G., Zhang, F., 2013. DNA targeting specificity of RNA-guided Cas9 nucleases. Nat. Biotechnol. 31 (9), 827–832.

Jin, L., Liu, Y., Sun, F., Collins, M.T., Blackwell, K., Woo, A.S., Reichenberger, E.J., Hu, Y., 2017. Three novel ANO5 missense mutations in Caucasian and Chinese families and sporadic cases with gnathodiaphyseal dysplasia. Sci. Rep. 7, 40935.

Keller, J., Catala-Lehnen, P., Huebner, A.K., Jeschke, A., Heckt, T., Lueth, A., Krause, M., Koehne, T., Albers, J., Schulze, J., Schilling, S., Haberland, M., Denninger, H., Neven, M., Hermans-Borgmeyer, I., Streichert, T., Breer, S., Barvencik, F., Levkau, B., Rathkolb, B., Wolf, E., Calzada-Wack, J., Neff, F., Gailus-Durner, V., Fuchs, H., de Angelis, M.H., Klutmann, S., Tsourdi, E., Hofbauer, L.C., Kleuser, B., Chun, J., Schinke, T., Amling, M., 2014. Calcitonin controls bone formation by inhibiting the release of sphingosine 1-phosphate from osteoclasts. Nat. Commun. 5, 5215.

Luther, J., Yorgan, T.A., Rolvien, T., Ulsamer, L., Koehne, T., Liao, N., Keller, D., Vollersen, N., Teufel, S., Neven, M., Peters, S., Schweizer, M., Trumpp, A., Rosigkeit, S., Bockamp, E., Mundlos, S., Kornak, U., Oheim, R., Amling, M., Schinke, T., David, J.P., 2018. Wnt1 is an Lrp5-independent bone-anabolic Wnt ligand. Sci. Transl. Med. 10 (466).

Marconi, C., Brunamonti Binello, P., Badiali, G., Caci, E., Cusano, R., Garibaldi, J., Pippucci, T., Merlini, A., Marchetti, C., Rhoden, K.J., Galietta, L.J., Lalatta, F., Balbi, P., Seri, M., 2013. A novel missense mutation in ANO5/TMEM16E is causative for gnathodiaphyseal dyplasia in a large Italian pedigree. Eur. J. Hum. Genet. 21 (6), 613–619.

Marechal, G., Schouman, T., Mauprivez, C., Benassarou, M., Chaine, A., Diner, P.A., Zazurca, F., Soupre, V., Michot, C., Baujat, G., Khonsari, R.H., 2019. Gnathodiaphyseal dysplasia with a novel R597I mutation of ANO5: mandibular reconstruction strategies. J. Stomatol. Oral Maxillofac. Surg. 120 (5), 428–431.

Mizuta, K., Tsutsumi, S., Inoue, H., Sakamoto, Y., Miyatake, K., Miyawaki, K., Noji, S., Kamata, N., Itakura, M., 2007. Molecular characterization of GDD1/TMEM16E, the gene product responsible for autosomal dominant gnathodiaphyseal dysplasia. Biochem. Biophys. Res. Commun. 357 (1), 126–132.

Nishiyama, K.K., Macdonald, H.M., Moore, S.A., Fung, T., Boyd, S.K., McKay, H.A., 2012. Cortical porosity is higher in boys compared with girls at the distal radius and distal tibia during pubertal growth: an HR-pQCT study. J. Bone Miner. Res. 27 (2), 273–282.

Otaify, G.A., Whyte, M.P., Gottesman, G.S., McAlister, W.H., Eric Gordon, J., Hollander, A., Andrews, M.V., El-Mofty, S.K., Chen, W.S., Veis, D.V., Stolina, M., Woo, A.S., Katsonis, P., Lichtarge, O., Zhang, F., Shinawi, M., 2018. Gnathodiaphyseal dysplasia: severe atypical presentation with novel heterozygous mutation of the anoctamin gene (ANO5). Bone 107, 161–171.

Ousingsawat, J., Wanitchakool, P., Kmit, A., Romao, A.M., Jantarajit, W., Schreiber, R., Kunzelmann, K., 2015. Anoctamin 6 mediates effects essential for innate immunity downstream of P2X7 receptors in macrophages. Nat. Commun. 6, 6245.

Pedemonte, N., Galietta, L.J., 2014. Structure and function of TMEM16 proteins (anoctamins). Physiol. Rev. 94 (2), 419–459.

Rolvien, T., Koehne, T., Kornak, U., Lehmann, W., Amling, M., Schinke, T., Oheim, R., 2017. A novel ANO5 mutation causing gnathodiaphyseal dysplasia with high bone turnover osteosclerosis. J. Bone Miner. Res. 32 (2), 277–284.

Schessl, J., Kress, W., Schoser, B., 2012. Novel ANO5 mutations causing hyper-CK-emia, limb girdle muscular weakness and Miyoshi type of muscular dystrophy. Muscle Nerve 45 (5), 740–742.

Schneider, C.A., Rasband, W.S., Eliceiri, K.W., 2012. NIH image to ImageJ: 25 years of image analysis. Nat. Methods 9 (7), 671–675.

Tsutsumi, S., Kamata, N., Vokes, T.J., Maruoka, Y., Nakakuki, K., Enomoto, S., Omura, K., Amagasa, T., Nagayama, M., Saito-Ohara, F., Inazawa, J., Moritani, M., Yamaoka, T., Inoue, H., Itakura, M., 2004. The novel gene encoding a putative transmembrane protein is mutated in gnathodiaphyseal dysplasia (GDD). Am. J. Hum. Genet. 74 (6), 1255–1261.

Wang, X., Liu, X., Dong, R., Liang, C., Reichenberger, E.J., Hu, Y., 2019. Genetic disruption of anoctamin 5 in mice replicates human gnathodiaphyseal dysplasia (GDD). Calcif. Tissue Int. 104 (6), 679–689.

Xu, J., El Refaey, M., Xu, L., Zhao, L., Gao, Y., Floyd, K., Karaze, T., Janssen, P.M., Han, R., 2015. Genetic disruption of Ano5 in mice does not recapitulate human ANO5-deficient muscular dystrophy. Skelet. Muscle 5, 43.

Yorgan, T.A., Peters, S., Jeschke, A., Benisch, P., Jakob, F., Amling, M., Schinke, T., 2015. The anti-osteoanabolic function of sclerostin is blunted in mice carrying a high bone mass mutation of Lrp5. J. Bone Miner. Res. 30 (7), 1175–1183.

Yu, K., Whitlock, J.M., Lee, K., Ortlund, E.A., Cui, Y.Y., Hartzell, H.C., 2015. Identification of a lipid scrambling domain in ANO6/TMEM16F. Elife 4, e06901.

Zeng, B., Liao, J., Zhang, H., Fu, S., Chen, W., Pan, G., Li, Q., Chen, W., Ferrone, S., Wu, B., Sun, S., Hu, J., Ahn, M.H., Lin, Z., Yu, D., Ou, Z., Wang, X., Mo, F., Huang, N., Hamilton, J.A., Li, J., Fan, S., 2019. Novel ANO5 mutation c.1067G > T (p.C356F) identified by whole genome sequencing in a big family with atypical gnathodiaphyseal dysplasia. Head Neck 41 (1), 230–238.